Measurements and calculations of 2*s*-2*p* transitions in neonlike germanium: Achieving agreement at the 10^{-4} level

P. Beiersdorfer,* G. V. Brown, N. Hell, T. Lockard, J. Nilsen, and D. Panchenko
Physics Division, Lawrence Livermore National Laboratory, Livermore, California 94550, USA

L. M. R. Hobbs and D. J. Hoarty
Physics Department, AWE plc, Reading RG7 4PR, England, United Kingdom

M. F. Gu
Space Sciences Laboratory, University of California, Berkeley, California 94720, USA

(Received 9 January 2019; revised manuscript received 19 June 2019; published 26 September 2019)

Calculations that achieve spectroscopic accuracy, i.e., at the level of 10^{-4} or better, are rare and typically restricted to few-electron systems. Here we present high-resolution grating spectrometer measurements of 11 $2s_{1/2}$-$2p_{3/2}$ transitions in neonlike Ge^{22+} that distinguish between two different implementations of the many-body perturbation theory (MBPT) method, including our own. The measurements show that our implementation of the MBPT method consistently achieves spectroscopic accuracy at the 10^{-4} level for all of the measured lines. Moreover, our calculations improve the 10^{-3} accuracy of prior MBPT calculations by an order of magnitude and allow us to make greatly improved predictions of the location of potential photopumped lines in Ge^{22+}. The measurements also improve on previous measurements of $2s_{1/2}$-$2p_{3/2}$ transitions in fluorinelike Ge^{23+} and oxygenlike Ge^{24+}. Measurements of $n = 2$ to $n = 3$ transitions in Al^{7+}, Al^{8+}, and Al^{9+} are used to support our measurement accuracy at the 10^{-5} level.

DOI: 10.1103/PhysRevA.100.032516

I. INTRODUCTION

Because of the $1s^22s^22p^6$ closed-shell ground-state configuration, neonlike ions are stable over a wide range of plasma temperatures, and, analogously to heliumlike ions, they emit intense x-ray lines. As a result, the L-shell x-ray emission from neonlike ions has been used as an important diagnostic of plasma parameters in magnetic fusion, inertial fusion, as well as solar physics and x-ray astronomy [1–8]. By contrast, intrashell transitions within neonlike ions, such as the 3*s*-3*p* transitions, are comparatively weak, but they have been playing an important role in the development of x-ray lasers [9,10]. Neonlike germanium has been one of the key elements in this ongoing effort [11–13]. Intrashell transitions within the $n = 3$ complex have also been studied as a means in extreme ultraviolet spectroscopy to measure the abundance of neonlike ions, especially that of neonlike iron [14]. In comparisons with solar measurements, resulting in findings later confirmed in laboratory measurements [15], the authors [14] showed that even the best available calculations differed from the measured values of some neonlike 3-3 lines by about 0.8 Å, or 0.4 % of the overall wavelength. This was well more than an order of magnitude larger than the percentage differences observed for the 2-3 x-ray transition of neonlike ions [16]. The large discrepancy even raised doubt on the proper identification of the 3-3 transitions.

Transitions within the $n = 2$ shell of excited neonlike ions are also weak and, compared with 2-3 or even 3-3 transitions, have received little experimental attention. However, they provide another opportunity for testing the accuracy of modern atomic structure calculations. The $(1s^22s_{1/2}2p^63s_{1/2})_{J=0} \rightarrow (1s^22s^22p^5_{3/2}3s_{1/2})_{J=1}$ intrashell transition was identified in neonlike uranium [17]. This U^{82+} transition is situated in the 4.6-keV x-ray region among several 2-2 transitions from more highly charged uranium ions. Theory at the time was able to predict the energy of the line only to within 0.2% or 8 eV. However, these 2-2 measurements stimulated new theoretical approaches [18,19], which resulted in much closer agreement with the measurements. The same $(1s^22s_{1/2}2p^63s_{1/2})_{J=0} \rightarrow (1s^22s^22p^5_{3/2}3s_{1/2})_{J=1}$ transition was subsequently identified among the 2-2 transitions of highly charged thorium [20]. However, a more recent measurement did not locate this transition among the 2-2 transitions of highly charged tungsten [21]. Our measurement of this and several other 2-2 transitions in neonlike germanium Ge^{22+}, thus, extends the prior observations from $Z = 90$ to $Z = 32$.

The 2-2 transitions of Ge^{22+} have been suggested as a possible diagnostic to test the efficacy of line transfer in photopumping schemes [22]. Such schemes make use of possible K- and L-shell line coincidences. In particular, because of a close wavelength coincidence [23] it appears possible to use the K-shell Lyman-α lines of hydrogenlike magnesium to excite the $(1s^22s^22p^6)_{J=0} \rightarrow (1s^22s_{1/2}2p^63p_{1/2})_{J=1}$ transition in neonlike germanium, i.e., to transfer population from the excited levels in hydrogenlike

*beiersdorfer1@llnl.gov

magnesium to the $(1s^2 2s_{1/2} 2p^6 3p_{1/2})_{J=1}$ level in neonlike germanium. The $(1s^2 2s_{1/2} 2p^6 3p_{1/2})_{J=1}$ level in neonlike germanium will decay in part via a $2p_{3/2} \rightarrow 2s_{1/2}$ transition to $(1s^2 2s^2 2p^5_{3/2} 3p_{1/2})_{J=2}$, which is the upper level of one of the neonlike germanium x-ray laser lines [23]. By measuring the enhancement of this $2p_{3/2} \rightarrow 2s_{1/2}$ transition it is, in principle, possible to assess the efficacy of the population transfer.

The neonlike $(1s^2 2s_{1/2} 2p^6 3p_{1/2})_{J=1} \rightarrow (1s^2 2s^2 2p^5_{3/2} 3p_{1/2})_{J=2}$ transition has not yet been experimentally identified, but its wavelength can be estimated from measurements of the $(1s^2 2s_{1/2} 2p^6 3p_{1/2})_{J=1} \rightarrow (1s^2 2s^2 2p^6)_{J=0}$ [23], the $(1s^2 2s^2 2p^5_{3/2} 3p_{1/2})_{J=2} \rightarrow (1s^2 2s^2 2p^5_{3/2} 3s_{1/2})_{J=1}$ [23], and the $(1s^2 2s^2 2p^5_{3/2} 3s_{1/2})_{J=1} \rightarrow (1s^2 2s^2 2p^6)_{J=0}$ [24] transitions. Using these measurements we get a value of 190.44 ± 0.64 eV for the energy difference of the $(1s^2 2s_{1/2} 2p^6 3p_{1/2})_{J=1}$ and $(1s^2 2s^2 2p^5_{3/2} 3p_{1/2})_{J=2}$ levels, or a wavelength of 65.10 ± 0.22 Å. The accuracy of this wavelength estimate is not sufficient to identify this line among a veritable forest of 2-2 lines in neonlike germanium that are predicted to exist between 61 and 68 Å, especially because the other 2-2 transitions are known only from calculations. Direct measurements of 2-2 transitions are needed not only to determine some of the lines in this forest but, most importantly, to assess theoretical approaches in the hope to identify those calculations that might have spectroscopic accuracy.

In the following we present measurements of several 2-2 transitions in neonlike germanium. Our experimental accuracy is sufficient to distinguish among the different predictions that rely on the many-body perturbation theory (MBPT) approach, which is among the most accurate theoretical methods for calculating the level energies of highly charged multielectron ions. We have also observed one 2-2 transition in fluorinelike and two 2-2 transitions in oxygenlike germanium. Unlike the neonlike transitions, the F-like and O-like ones have been identified before [25–28], and we improve on the prior measurement accuracy.

We also present wavelength calculations using the Flexible Atomic Code (FAC) [29] and the MBPT option of FAC [30], as well as collisional radiative modeling calculations with FAC that predict spectral intensities. The wavelengths calculated with FAC differ from experiment by 1 Å or more, and they are too inaccurate to identify the observed lines. However, calculating the neonlike germanium lines with FAC-MBPT produces remarkable agreement with the observations. In fact, the predicted wavelengths are essentially in perfect agreement with measurements. By contrast, we show that earlier predictions using a different implementation of the MBPT method are about an order of magnitude less accurate.

II. CALCULATIONS

Calculations of the energies of the 36 possible excited states in Ge^{22+} produced by promoting an electron with principal quantum number $n = 2$ in the ground level to the $n = 3$ shell were carried out using the MBPT option in FAC. The details of the MBPT method as implemented in FAC have been described in [30]. The $1s^2 2\ell^8$ and $1s^2 2\ell^7 3\ell'$ states are included in the configuration-interaction expansion that defines the reference space. Electron correlations with the orthogonal space are treated in the second-order MBPT by diagonalizing the effective Hamiltonian matrix within the reference space, the matrix elements of which contain the second-order MBPT corrections. The radial basis functions used to construct the orthogonal space are derived from the solutions to the Dirac equation of a model potential, which is optimized for the Ge^{22+} ground state by minimizing its energy. The wave functions are contained in a spherical box with radius determined such that all $n \leqslant 3$ orbitals have negligible amplitudes outside the box. Such a boundary condition discretizes the continuum so that correlation effects can be included without complications of integrating over the orbitals in the continuum spectrum. The Breit interaction is included in the frequency independent limit. Lamb shifts due to vacuum polarization and self-energy corrections are computed using the model QED operator of Shabaev, Tupitsyn, and Yerokhin [31].

The results of the calculations are given in Table I. Here we compare our numbers with those generated by Safronova *et al.* [32], who also employed the MBPT method. The MBPT method employed in our work is in principle very similar to that of Ref. [32], and this is reflected in the excellent agreement for the majority of level energies produced by the two calculations. However, there are several levels for which the differences are between -0.39 and $+0.31$ eV. In one case, i.e., level 35 or $(1s^2 2s_{1/2} 2p^6 3d_{5/2})_{J=3}$, the difference is as large as 2.6 eV. It is not immediately clear what may have caused such large differences. In Table I, we also list the second-order corrections of Coulomb and Breit interactions, and Lamb shifts of the levels.

Unfortunately, Ref. [32] listed individual correction terms only for Ne-like molybdenum. Therefore, we have performed a similar calculation of Ne-like Mo in order to compare with the results of Ref. [32], as shown in Table II. We see a similar pattern of excellent agreement for most levels. There are some levels for which the difference is between ± 0.25 eV, but level 35 is once again a clear outlier, with our result being 2.3 eV lower.

The Lamb shifts in both calculations agree to within about 0.05 eV, so we can rule out that being the source of discrepancy. The second-order corrections to the Coulomb and Breit terms differ in the two calculations, but this is understandable as the zeroth-order potential used here is different from that of Ref. [32]. Our second-order corrections are generally slightly smaller than those of Ref. [32], reflecting a slightly better zeroth-order potential. However, the exact partitioning of zeroth-order and perturbation potentials should not be important once the perturbation series have converged. Indeed, by varying our zeroth-order potential (e.g., by optimizing the potential to minimize the averaging energy of the $2l^7 3l'$ configurations instead of the ground state), we observe that the final level energies vary typically on the order of 0.1 eV for both Mo and Ge, which can be considered a measure of theoretical uncertainty in our calculations. The discrepancy for level 35 therefore far exceeds an amount that can be attributed to the difference in the zeroth-order potential.

We point out one peculiar trend in the Ne-like Mo energies of Ref. [32]: the second-order corrections of the Coulomb and

TABLE I. Comparison of the energies of the lowest 36 excited levels of neonlike Ge^{22+} calculated by the MBPT module in the Flexible Atomic Code with the MBPT values calculated by Safronova *et al.* [32]. In the last three columns, we list the second-order corrections to the Coulomb energy ($E^{(2)}$), Breit interaction ($B^{(2)}$), and Lamb shifts ($E_{\rm Lamb}$).

Level index	Configuration	E[a] (eV)	E[b] (eV)	ΔE (eV)	ΔE (ppm)	$E^{(2)}$ (eV)	$B^{(2)}$ (eV)	$E_{\rm Lamb}$ (eV)
0	$(1s^22s^22p_{1/2}^22p_{3/2}^4)_0$	0.00000	0.00000	0.00000	0	0.000	0.000	0.000
1	$(1s^22s^22p_{1/2}^22p_{3/2}^33s_{1/2})_2$	1235.58437	1235.63708	−0.05271	−43	1.776	0.246	0.155
2	$(1s^22s^22p_{1/2}^22p_{3/2}^33s_{1/2})_1$	1238.24107	1238.27273	−0.03166	−26	1.628	0.244	0.156
3	$(1s^22s^22p_{1/2}2p_{3/2}^43s_{1/2})_0$	1268.12154	1268.13333	−0.01179	−9	1.777	0.254	0.229
4	$(1s^22s^22p_{1/2}2p_{3/2}^43s_{1/2})_1$	1269.51873	1269.53299	−0.01426	−11	1.679	0.252	0.229
5	$(1s^22s^22p_{1/2}^22p_{3/2}^33p_{1/2})_1$	1278.29987	1278.52891	−0.22904	−179	1.757	0.229	−0.063
6	$(1s^22s^22p_{1/2}^22p_{3/2}^33p_{1/2})_2$	1281.60337	1281.60967	−0.00630	−5	1.610	0.228	−0.063
7	$(1s^22s^22p_{1/2}^22p_{3/2}^33p_{3/2})_3$	1287.68798	1287.68911	−0.00113	−1	1.676	0.232	−0.047
8	$(1s^22s^22p_{1/2}^22p_{3/2}^33p_{3/2})_1$	1288.51703	1288.25089	0.26614	207	1.581	0.230	−0.050
9	$(1s^22s^22p_{1/2}^22p_{3/2}^33p_{3/2})_2$	1291.71985	1291.71240	0.00745	6	1.590	0.226	−0.047
10	$(1s^22s^22p_{1/2}^22p_{3/2}^33p_{3/2})_0$	1302.84219	1302.74444	0.09775	75	0.864	0.202	−0.030
11	$(1s^22s^22p_{1/2}2p_{3/2}^43p_{1/2})_1$	1313.09698	1313.08988	0.00710	5	1.611	0.237	0.011
12	$(1s^22s^22p_{1/2}2p_{3/2}^43p_{3/2})_1$	1321.18957	1321.08575	0.10382	79	1.654	0.237	0.024
13	$(1s^22s^22p_{1/2}2p_{3/2}^43p_{3/2})_2$	1322.11927	1322.05320	0.06607	50	1.617	0.236	0.028
14	$(1s^22s^22p_{1/2}2p_{3/2}^43p_{1/2})_0$	1333.09534	1332.78550	0.30984	232	−2.313	0.085	−0.003
15	$(1s^22s^22p_{1/2}^22p_{3/2}^33d_{3/2})_0$	1342.26832	1342.25605	0.01227	9	1.747	0.239	−0.066
16	$(1s^22s^22p_{1/2}^22p_{3/2}^33d_{3/2})_1$	1343.98379	1344.17359	−0.18980	−141	1.706	0.237	−0.064
17	$(1s^22s^22p_{1/2}^22p_{3/2}^33d_{5/2})_4$	1346.91162	1346.96460	−0.05298	−39	1.573	0.241	−0.060
18	$(1s^22s^22p_{1/2}^22p_{3/2}^33d_{5/2})_2$	1347.17340	1347.26600	−0.09260	−69	1.633	0.238	−0.061
19	$(1s^22s^22p_{1/2}^22p_{3/2}^33d_{3/2})_3$	1347.27372	1347.30506	−0.03134	−23	1.432	0.234	−0.062
20	$(1s^22s^22p_{1/2}^22p_{3/2}^33d_{3/2})_2$	1349.98535	1350.04164	−0.05629	−42	1.405	0.234	−0.061
21	$(1s^22s^22p_{1/2}^22p_{3/2}^33d_{5/2})_3$	1352.01655	1352.09308	−0.07653	−57	1.400	0.238	−0.059
22	$(1s^22s^22p_{1/2}^22p_{3/2}^33d_{5/2})_1$	1360.33219	1360.15032	0.18187	134	0.674	0.241	−0.047
23	$(1s^22s^22p_{1/2}2p_{3/2}^43d_{3/2})_2$	1379.46466	1379.45850	0.00616	4	1.472	0.241	0.011
24	$(1s^22s^22p_{1/2}2p_{3/2}^43d_{5/2})_2$	1381.19399	1381.08852	0.10547	76	1.547	0.242	0.012
25	$(1s^22s^22p_{1/2}2p_{3/2}^43d_{5/2})_3$	1382.26867	1382.29042	−0.02175	−16	1.419	0.247	0.015
26	$(1s^22s^22p_{1/2}2p_{3/2}^43d_{3/2})_1$	1390.01478	1390.02828	−0.01350	−10	0.029	0.257	0.015
27	$(1s^22s_{1/2}2p_{1/2}^22p_{3/2}^43s_{1/2})_1$	1426.61003	1426.72016	−0.11013	−77	−0.800	0.126	−0.647
28	$(1s^22s_{1/2}2p_{1/2}^22p_{3/2}^43s_{1/2})_0$	1434.90581	1434.93447	−0.02866	−20	−1.936	0.090	−0.652
29	$(1s^22s_{1/2}2p_{1/2}^22p_{3/2}^43p_{1/2})_0$	1471.26655	1471.28194	−0.01539	−10	−0.972	0.100	−0.869
30	$(1s^22s_{1/2}2p_{1/2}^22p_{3/2}^43p_{1/2})_1$	1472.03068	1472.18343	−0.15275	−104	−0.989	0.101	−0.867
31	$(1s^22s_{1/2}2p_{1/2}^22p_{3/2}^43p_{3/2})_2$	1478.96803	1479.05488	−0.08685	−59	−0.956	0.104	−0.853
32	$(1s^22s_{1/2}2p_{1/2}^22p_{3/2}^43p_{3/2})_1$	1481.40074	1481.37388	0.02686	18	−0.983	0.105	−0.852
33	$(1s^22s_{1/2}2p_{1/2}^22p_{3/2}^43d_{3/2})_1$	1535.44070	1535.43682	0.00388	3	−1.181	0.115	−0.873
34	$(1s^22s_{1/2}2p_{1/2}^22p_{3/2}^43d_{3/2})_2$	1535.90667	1536.29244	−0.38577	−251	−1.163	0.114	−0.872
35	$(1s^22s_{1/2}2p_{1/2}^22p_{3/2}^43d_{5/2})_3$	1536.83666	1539.43135	−2.59469	−1688	−1.122	0.118	−0.871
36	$(1s^22s_{1/2}2p_{1/2}^22p_{3/2}^43d_{5/2})_2$	1543.55109	1543.23940	0.31169	202	−1.517	0.112	−0.871

[a]Present work.

[b]Ref. [32] and private communication.

Breit interaction for level 35 appear to be very different from the neighboring levels, which are of the same 2*s*3*d* configurations but which have a different total angular momentum. For example, Safronova *et al.* [32] calculate $B^{(2)} \approx 0.55$ eV for each of these levels, but $B^{(2)} = -0.09$ eV for level 35. In our calculation the correction terms to these energies all have the same value within ∼0.01 eV. However, ultimately only experiment can resolve which of the two calculations, if any, is close to the actual energy.

In addition to the FAC-MBPT calculations, we also performed the usual FAC calculation without involving the MBPT option. These calculations are expected to be of lower accuracy, and we list the specific transition wavelengths calculated with FAC in Table III together with the values from our FAC-MBPT and the Safronova *et al.* [32] calculations.

We have also used FAC to generate a collisional-radiative model to predict the expected line intensities of the 2-2 transitions in Ge^{22+}. The first model involves all 36 excited levels with an $n = 3$ valence electron. The second model includes all levels with an $n \leqslant 5$ valence electron and, therefore, includes more radiative cascade contributions than the first model. Indeed, radiative cascades from the high-lying levels significantly increase the predicted intensities for many (but not all) lines. Indirect line excitation processes [33] may further add to the predicted intensities, but they are not included in our present models. We use the calculated intensities together with the FAC-MBPT produced wavelengths to generate a

TABLE II. Comparison of the energies and individual correction terms of the lowest 36 excited levels of neonlike Mo^{32+} calculated by the MBPT module in the Flexible Atomic Code with the MBPT values calculated by Safronova *et al.* [32].

Level index	$E^{(2)}$[a] (eV)	$E^{(2)}$[b] (eV)	$B^{(2)}$[a] (eV)	$B^{(2)}$[b] (eV)	$E_{\rm Lamb}$[a] (eV)	$E_{\rm Lamb}$[b] (eV)	$E_{\rm tot}$[a] (eV)	$E_{\rm tot}$[b] (eV)	ΔE (eV)
1	1.550	−2.182	0.444	0.716	0.413	0.370	2376.821	2376.804	0.017
2	1.394	−2.180	0.440	0.713	0.414	0.370	2380.714	2380.682	0.033
3	1.462	−2.340	0.407	0.735	−0.203	−0.185	2441.237	2441.357	−0.121
4	1.377	−2.272	0.406	0.718	−0.201	−0.182	2443.979	2444.032	−0.053
5	1.449	−2.348	0.417	0.694	−0.149	−0.139	2469.466	2469.483	−0.017
6	1.384	−2.446	0.415	0.702	−0.153	−0.141	2469.626	2469.557	0.069
7	1.371	−2.182	0.407	0.697	−0.149	−0.139	2475.337	2475.358	−0.021
8	1.533	−2.416	0.475	0.743	0.635	0.580	2486.342	2486.224	0.118
9	1.449	−2.460	0.471	0.724	0.636	0.580	2488.167	2488.017	0.150
10	−0.351	−2.754	0.300	0.669	−0.134	−0.128	2497.066	2497.184	−0.119
11	1.501	−2.805	0.427	0.759	−0.212	−0.193	2547.369	2547.411	−0.042
12	1.447	−2.555	0.421	0.707	−0.209	−0.190	2550.702	2550.644	0.058
13	1.368	−2.601	0.442	0.737	0.023	0.027	2551.761	2551.689	0.072
14	1.176	−2.691	0.417	0.694	−0.207	−0.188	2554.522	2554.579	−0.057
15	1.319	−2.580	0.417	0.713	−0.205	−0.185	2556.580	2556.630	−0.051
16	1.350	−2.708	0.432	0.683	−0.195	−0.169	2557.793	2557.844	−0.051
17	1.207	−2.612	0.424	0.705	−0.198	−0.174	2560.955	2561.066	−0.111
18	1.178	−2.463	0.425	0.697	−0.194	−0.169	2565.501	2565.586	−0.085
19	−1.435	−3.333	0.232	0.678	0.011	0.016	2575.482	2575.597	−0.114
20	1.439	−2.634	0.443	0.727	0.066	0.063	2579.880	2579.700	0.180
21	0.019	−2.721	0.436	0.716	−0.176	−0.169	2579.888	2580.106	−0.217
22	1.378	−2.536	0.442	0.705	0.077	0.073	2581.595	2581.488	0.107
23	1.213	−2.958	0.447	0.718	0.019	0.024	2663.372	2663.326	0.045
24	1.326	−2.917	0.450	0.707	0.025	0.035	2669.630	2669.487	0.143
25	1.176	−2.860	0.460	0.707	0.032	0.044	2671.547	2671.509	0.038
26	0.111	−2.903	0.467	0.716	0.018	0.008	2677.048	2677.054	−0.006
27	−0.905	−3.641	0.234	0.563	−1.695	−1.815	2709.960	2709.983	−0.023
28	−2.051	−4.027	0.170	0.542	−1.710	−1.834	2722.419	2722.397	0.022
29	−1.092	−3.927	0.182	0.566	−2.321	−2.381	2775.412	2775.405	0.008
30	−1.126	−3.763	0.185	0.552	−2.314	−2.376	2776.704	2776.762	−0.059
31	−1.067	−3.867	0.191	0.533	−2.268	−2.335	2803.195	2803.223	−0.027
32	−1.089	−3.788	0.193	0.531	−2.269	−2.340	2806.350	2806.347	0.003
33	−1.320	−4.487	0.207	0.569	−2.336	−2.395	2884.111	2884.090	0.021
34	−1.309	−4.125	0.204	0.533	−2.334	−2.392	2885.622	2885.875	−0.252
35	−1.222	−1.480	0.216	−0.090	−2.324	−2.378	2889.942	2892.220	−2.279
36	−1.626	−4.378	0.205	0.550	−2.326	−2.381	2899.286	2899.037	0.249

[a]Present work.
[b]Ref. [32].

synthetic spectrum for comparison with our measurements. These predictions are shown in Fig. 1.

III. EXPERIMENT

The present experiment was performed at the EBIT-I ("Ebit-one") electron-beam ion trap at the Lawrence Livermore National Laboratory [34,35]. Injection of Ge into the ion trap was achieved by the evaporation of germanium(IV)ethoxide, which is similar to the injection method used at other facilities [36]. The germanium ionization balance was monitored using the EBIT Calorimeter Spectrometer, which is an x-ray microcalorimeter with about 5-eV resolution and full x-ray coverage from about 200 to 10 000 eV [37–39].

Because the lines of present interest fall into the 60–70-Å wavelength band, we employed one of the two available high-resolution grazing-incidence spectrometers [40,41] for our measurements. These instruments have been used before in the high-resolution measurements of the 2-2 extreme ultraviolet lines of very highly charged ions [42–44]. The particular instrument used for the present measurements [41] utilizes a gold-coated, $R = 44.3$-m grating with a variable line spacing centered around 2400 ℓ/mm and reflecting at about 2.5°. The roughly 50-μm-wide EBIT-I electron beam acts as the entrance slit for the otherwise slitless instrument. A cryogenically cooled, back-illuminated charge-coupled device camera with 1340 × 1300 20-μm-wide pixels is used for photon detection.

In order to establish the wavelength scale for the present measurements, we injected trimethyl borate. This compound was also used in our earlier measurement of the 2-2 lines of lithiumlike and berylliumlike praeseodymium [43], and here we employed the $1s2p\,^1P_1 \rightarrow 1s^2\,^1S_0$ resonance transition of

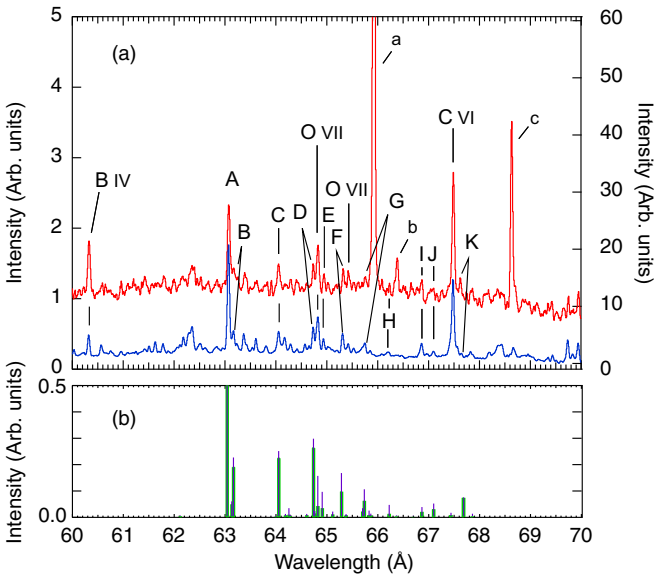

FIG. 1. (a) Spectra measured at the Livermore EBIT-I facility below (blue, lower trace, $E_{\rm beam} = 2.0$ keV, right axis) and above the beam energy for ionizing Ge^{22+} (red, higher trace, $E_{\rm beam} = 2.7$ keV, left axis). The Ge^{22+} lines are labeled "A"–"G" (see Table II); the Ge^{23+} and Ge^{24+} lines are labeled "a"–"c" (see Table III). Reference lines from heliumlike B^{3+} (detected in first order), heliumlike O^{6+} (detected in third order), and hydrogenlike C^{5+} (detected in second order) are denoted "B IV," "O VII," and "C VI," respectively. (b) Predicted intensities and line positions from our FAC-MBPT calculations. The wide (green) lines are from our $n = 3$ model; the narrow (blue) lines are from our $n \leqslant 5$ model. The intensity of the strongest line predicted by each model is set to unity.

heliumlike B^{3+} as a reference line. Its wavelength of 60.3138 Å is given to high accuracy by the calculations of Drake [45]. Injection of carbon dioxide provided the $1s2p\,^1P_1 \rightarrow 1s^2\,^1S_0$ and $1s2p\,^3P_1 \rightarrow 1s^2\,^1S_0$ resonance and intercombination lines of heliumlike O^{6+} at 64.8045 and 65.4109 Å, respectively, in third-order reflection [45] and the $2p \rightarrow 1s$ Lyman-α transitions of hydrogenlike C^{5+} at 67.4710 Å in second-order reflection [46].

Germanium spectra were recorded at several electron-beam energies. Setting the beam energy to about 2.7 keV allowed for the production not only of neonlike but also of fluorinelike and oxygenlike germanium. Setting the beam energy to values below the 2.18-keV ionization potential of Ge^{22+} assured that the spectra were free of contributions from fluorinelike and oxygenlike germanium. Spectra from those two run conditions are shown in Fig. 1.

The spectra observed at beam energies above the ionization potential are dominated by the $(1s^22s_{1/2}2p^6)_{J=1/2} \rightarrow (1s^22s^22p^5_{3/2})_{J=3/2}$ transition in fluorinelike Ge^{23+}. This line is labeled "a" in Fig. 1. We also see two lines from oxygenlike Ge^{24+}, which are labeled "b" and "c". These correspond to the $(1s^22s_{1/2}2p^5_{3/2})_{J=2} \rightarrow (1s^22s^22p^2_{1/2}2p^2_{3/2})_{J=2}$ and $(1s^22s_{1/2}2p^5_{3/2})_{J=1} \rightarrow (1s^22s^22p^2_{1/2}2p^2_{3/2})_{J=2}$ transitions.

Fluorinelike line a has been observed in previous measurements [25,27,28], and the wavelength of 65.906 ± 0.003 Å that we determine for this line is in excellent agreement with the earlier measurements, albeit somewhat more accurate. The two oxygenlike lines have also been measured before [25,27,28]. However, the agreements both among the earlier measurements and with our results are not as good as for the fluorinelike line, as there is substantial scatter among the previous measurements. The comparison between our measurements and the earlier results is given in Table IV.

The spectra recorded at a beam energy of 2.0 keV, which is below the energy to produce fluorinelike Ge^{23+} ions, are devoid of lines a–c, as is expected. The sum of eight such spectra recorded for 30 min each is shown in Fig. 1. These spectra exhibit a plethora of weak features, the strongest of which are also seen in the higher-energy spectra. An identification of the Ge^{22+} lines among these features would have been impossible without the predictions from our FAC-MBPT calculations. A comparison between these predictions and the measurements, however, readily enables identification of the four strongest Ge^{22+} lines, as both the wavelengths and relative intensities match well. These lines are labeled "A"–"D" in Fig. 1.

Encouraged by the excellent wavelength match of theory and measurement for the four strongest neonlike lines, we have identified seven additional Ge^{22+} lines. These three lines are labeled "E"–"K," and they are considerably weaker than the first four lines. However, we find matching features in both sets of spectra and assign those features to the corresponding transitions in the calculations. The intensity of the feature associated with line K, however, varies considerably between the spectra above and below the ionization potential of Ge^{22+}. This indicates that the line is either blended with an unknown line or incorrectly identified. We, therefore, consider this a tentative identification. An overview of the 11 neonlike lines identified in our spectra is given in Table III.

Although we noticed slight shifts from day to day in the position of the reference lines, these did not affect the accuracy of our measurements because the same reference lines also appeared in the germanium spectra. This can be seen in Fig. 1, where we have labeled the B^{3+}, C^{5+}, and O^{6+} reference lines by their spectroscopic notation "B IV," "C VI," and "O VII," respectively. Our wavelength calibration could reproduce all of these lines to within less than 3 mÅ. These lines have intensities similar to the strongest neonlike germanium lines, and we thus expect the same accuracy for the germanium lines. As a result, we have assigned 3-mÅ uncertainties to the strongest measured neonlike lines; the uncertainties of the weakest lines are considerably larger, however. Moreover, the uncertainties of lines G and K are given by possible blending with other weak features.

Several weeks after the original germanium measurements we used our setup to record spectra of aluminum and additional spectra of germanium. The germanium spectra provided the reference lines to calibrate the aluminum spectra. A sample aluminum spectrum is shown in Fig. 2. The spectrum is dominated by the known lines of Al^{7+} and Al^{8+} [47]. Although we used the germanium lines as the reference lines, we could reproduce the wavelengths of the strongest aluminum lines given by Kelly [48] to within 5 mÅ. This again affirms the overall accuracy of our measurements.

TABLE III. Comparison of measured and calculated wavelengths of neonlike Ge^{22+} lines identified in the present measurements. The lines are labeled in the notation used in Fig. 1. I denotes the line intensity; $\Delta\lambda$ is defined as the difference between experimental and calculated wavelengths.

Key	Transition	I_{exp}	I[a]	λ_{exp} (Å)	λ[a] (Å)	$\Delta\lambda$ (mÅ)	λ[b] (Å)	$\Delta\lambda$ (mÅ)	λ[c] (Å)	$\Delta\lambda$ (mÅ)
A	$(1s^22s_{1/2}2p^63s_{1/2})_{J=0} \rightarrow (1s^22s^22p^5_{3/2}3s_{1/2})_{J=1}$	1.00	1.00	63.058 ± 0.003	61.834	1224	63.043	15	63.044	14
B	$(1s^22s_{1/2}2p^63d_{5/2})_{J=2} \rightarrow (1s^22s^22p^5_{3/2}3d_{3/2})_{J=3}$	0.22[d]	0.23	63.155 ± 0.003	61.241	1914	63.168	−13	63.278	−123
	$(1s^22s_{1/2}2p^63d_{5/2})_{J=2} \rightarrow (1s^22s^22p^5_{3/2}3d_{5/2})_{J=2}$		0.06		61.184	1971	63.136	19	63.266	−111
C	$(1s^22s_{1/2}2p^63d_{5/2})_{J=2} \rightarrow (1s^22s^22p^5_{3/2}3d_{3/2})_{J=2}$	0.23	0.25	64.049 ± 0.003	63.087	968	64.053	−4	64.175	−126
D	$(1s^22s_{1/2}2p^63d_{5/2})_{J=2} \rightarrow (1s^22s^22p^5_{3/2}3d_{5/2})_{J=3}$	0.21	0.30	64.719 ± 0.003	63.741	978	64.732	−13	64.864	−145
E	$(1s^22s_{1/2}2p^63s_{1/2})_{J=1} \rightarrow (1s^22s^22p^5_{3/2}3s_{5/2})_{J=2}$	0.11	0.09	64.929 ± 0.010	63.956	973	64.909	20	64.885	44
F	$(1s^22s_{1/2}2p^63d_{5/2})_{J=3} \rightarrow (1s^22s^22p^5_{3/2}3d_{5/2})_{J=4}$	0.19	0.17	65.305 ± 0.005	64.310	995	65.281	24	64.419	886
G	$(1s^22s_{1/2}2p^63d_{3/2})_{J=2} \rightarrow (1s^22s^22p^5_{3/2}3d_{3/2})_{J=3}$	0.10	0.10	65.741 ± 0.020	64.724	1017	65.728	13	65.604	137
H	$(1s^22s_{1/2}2p^63p_{3/2})_{J=2} \rightarrow (1s^22s^22p^5_{3/2}3p_{3/2})_{J=2}$	0.03	0.04	66.205 ± 0.030	65.207	998	66.214	−9	66.181	24
I	$(1s^22s_{1/2}2p^63p_{3/2})_{J=2} \rightarrow (1s^22s^22p^5_{3/2}3p_{3/2})_{J=2}$	0.11	0.04	66.844 ± 0.010	65.791	1053	66.876	−32	66.854	−10
J	$(1s^22s_{1/2}2p^63d_{5/2})_{J=3} \rightarrow (1s^22s^22p^5_{3/2}3d_{5/2})_{J=3}$	0.04	0.05	67.076 ± 0.030	66.029	1047	67.084	−8	66.182	894
K	$(1s^22s_{1/2}2p^63d_{5/2})_{J=2} \rightarrow (1s^22s^22p^5_{3/2}3d_{5/2})_{J=1}$	0.15	0.07	67.620 ± 0.030	66.684	936	67.670	−50	67.718	−98

[a]Present FAC calculations.
[b]Present FAC-MBPT calculations.
[c]MBPT calculations based on the energy-level values from Ref. [32].
[d]Blend.

IV. COMPARISON OF EXPERIMENT AND THEORY

An overview of the 11 neonlike lines identified in our spectra is given in Table III. This table compares the wavelengths inferred from our measurements with the wavelengths from our FAC and FAC-MBPT calculations as well as those from MBPT calculations by Safronova *et al.* [32].

The strongest line, labeled "A" in Fig. 1 and Table III, corresponds to the $(1s^22s_{1/2}2p^63s_{1/2})_{J=0} \rightarrow (1s^22s^22p^5_{3/2}3s_{1/2})_{J=1}$ transition. This line has been observed before in the spectra of neonlike Th^{80+} and U^{82+} [17,20], where it was the only neonlike line identified among the $2p_{3/2} \rightarrow 2s_{1/2}$ transitions from higher (fluorinelike through lithiumlike) charge states of thorium and uranium.

Both MBPT predictions agree with the measured values of line A within 15 mÅ. By contrast, the FAC predictions differ by over 1 Å, and similarly large discrepancies can be noted for the other ten neonlike Ge^{22+} lines in Table III calculated with FAC. The excellent agreement noted for both MBPT calculations for line A no longer holds for most of the other neonlike lines. The FAC-MBPT results agree within ±20 mÅ for eight lines and within ±50 mÅ for the remaining three lines in our measurements. The other MBPT predictions agree within ±20 mÅ for only one line and within ±50 mÅ for two additional lines. The remaining eight lines differ by more than ±100 mÅ and up to ±900 mÅ. The difference is, thus, almost an order of magnitude larger than that for the FAC-MBPT predictions.

We find the biggest difference between the MBPT calculations and the measured value for lines F and J, which correspond to the $(1s^22s_{1/2}2p^63d_{5/2})_{J=3} \rightarrow (1s^22s^22p^5_{3/2}3d_{5/2})_{J=4}$ and $(1s^22s_{1/2}2p^63d_{5/2})_{J=3} \rightarrow (1s^22s^22p^5_{3/2}3d_{5/2})_{J=3}$ transitions, respectively. Here, the differences are almost 1 Å, i.e., comparable to the difference observed for the FAC calculations. We have already noted that the energy of the $(1s^22s_{1/2}2p^63d_{5/2})_{J=3}$ common upper level (level 35 in Table I) calculated by Safronova *et al.* [32] differs by 2.6 eV from that calculated with FAC-MBPT. It is, thus, not surprising that the wavelength of a transition involving this level also shows a large difference.

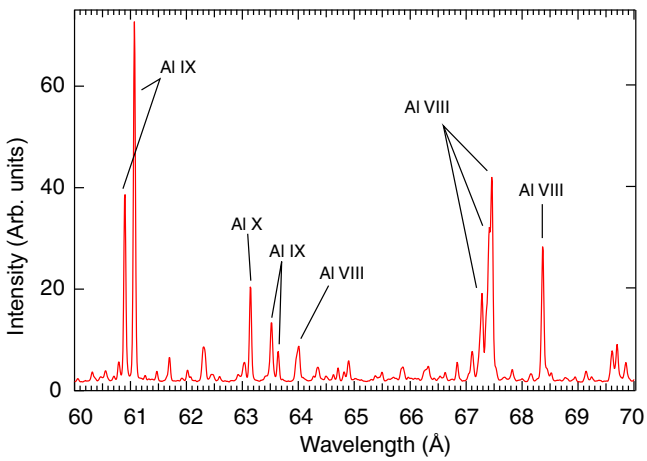

FIG. 2. Aluminum emission lines measured at the Livermore EBIT-I facility. The strongest lines are labeled by the associated aluminum ion state.

V. CONCLUSION

Our spectral measurements of highly charged germanium ions have yielded 11 features that we identify as Ge^{22+} lines. The measured wavelengths of these features are essentially in perfect agreement with our FAC-MBPT calculations. The difference with earlier MBPT predictions is about an order of magnitude more, and for two lines the difference is almost two orders of magnitude larger than that achieved with our calculations. Although we do not know why the two implementations of the MBPT method deliver such different results,

TABLE IV. Comparison of the wavelengths of fluorinelike Ge^{23+} and oxygenlike Ge^{24+} lines identified in the present measurements with those reported earlier. The lines are labeled in the notation used in Fig. 1.

Key	Transition	λ[a] (Å)	λ[b] (Å)	λ[c] (Å)	λ[d] (Å)
		Ge XXIV			
a	$(1s^2 2s_{1/2} 2p^6)_{J=1/2} \rightarrow (1s^2 2s^2 2p^5_{3/2})_{J=3/2}$	65.906 ± 0.003	65.902 ± 0.010	65.893 ± 0.005	65.930 ± 0.010
		Ge XXV			
b	$(1s^2 2s_{1/2} 2p^5_{3/2})_{J=2} \rightarrow (1s^2 2s^2 2p^2_{1/2} 2p^2_{3/2})_{J=2}$	66.366 ± 0.003	66.372 ± 0.010	66.364 ± 0.005	66.390 ± 0.010
c	$(1s^2 2s_{1/2} 2p^5_{3/2})_{J=1} \rightarrow (1s^2 2s^2 2p^2_{1/2} 2p^2_{3/2})_{J=2}$	68.638 ± 0.003	68.619 ± 0.010	68.616 ± 0.005	68.650 ± 0.010

[a]Present work.
[b]Ref. [28].
[c]Ref. [27].
[d]Ref. [25]

it is clear that highly accurate experiments are needed to tell them apart. The issue that causes such widely differing results, which is especially large for the energy of the $J = 3$ level in the two neonlike ions studied here, may also affect the accuracy of the calculations of levels in ionic systems other than neonlike ions. It will, thus, be of great importance for future investigations to uncover the cause for the problems we have noted.

Unfortunately, we cannot directly measure the $(1s^2 2s_{1/2} 2p^6 3p_{1/2})_{J=1} \rightarrow (1s^2 2s^2 2p^5_{3/2} 3p_{1/2})_{J=2}$ transition that plays an important role in line transfer studies [22,23]. In the absence of photopumping, our collisional-radiative model predicts this line to be about 25 times weaker than the strongest neonlike germanium line, line A. The line is, thus, too weak to unequivocally observe in our measurements. However, using our calculations we can make an estimate of its wavelength that is more accurate than what was done before.

Our FAC-MBPT calculations predict that the wavelength of the $(1s^2 2s_{1/2} 2p^6 3p_{1/2})_{J=1} \rightarrow (1s^2 2s^2 2p^5_{3/2} 3p_{1/2})_{J=2}$ transition (i.e., from level 30 to level 6) is 65.108 Å. Based on the consistently excellent agreement between our measurements and calculations we can assume an uncertainty of about 20 mÅ in this value. The estimated value of 65.108 ± 0.020 Å again compares very well with the value of 65.10 ± 0.22 Å derived from indirect measurements of the line, as stated in the Introduction. The uncertainty in our calculated value, however, is an order of magnitude lower. From the energy levels calculated by Safronova *et al.* [32] we can infer a value of 65.058 Å. From our measurements we can infer an uncertainty of about 0.140 Å in this value, which is only a slight improvement over the previous estimate of 65.10 ± 0.22 Å and seven times less accurate than our FAC-MBPT result.

The accuracy achieved in the FAC-MBPT calculations bodes well for applying this method to other systems, such as neonlike iron, where particular lines either cannot be measured directly or cannot be identified with current experimental techniques.

ACKNOWLEDGMENTS

We are grateful to Dr. U. Safronova for making her numerical results available to us. This work was performed under the auspices of the U.S. Department of Energy by Lawrence Livermore National Laboratory under Contract No. DE-AC52-07NA27344. The development of the enhanced MBPT module in FAC was supported in part by NASA's Astrophysics and Analysis Program under Contract No. NNG14WF24I.

[1] J. H. Parkinson, Astron. Astrophys. **24**, 215 (1973).
[2] B. W. Smith, J. C. Raymond, J. B. Mann, and R. D. Cowan, Astrophys. J. **298**, 898 (1985).
[3] P. Beiersdorfer, S. von Goeler, M. Bitter, K. W. Hill, R. A. Hulse, and R. S. Walling, Rev. Sci. Instrum. **60**, 895 (1989).
[4] C. J. Keane, B. A. Hammel, A. L. Osterheld, and D. R. Kania, Phys. Rev. Lett. **72**, 3029 (1994).
[5] F. B. S. Paerels and S. M. Kahn, Ann. Rev. Astron. Astrophys. **41**, 291 (2003).
[6] M. F. Gu, R. Gupta, J. R. Peterson, M. Sako, and S. M. Kahn, Astrophys. J. **649**, 979 (2006).
[7] P. Beiersdorfer, J. Clementson, J. Dunn, M. F. Gu, K. Morris, Y. Podpaly, E. Wang, M. Bitter, R. Feder, K. W. Hill, D. Johnson, and R. Barnsley, J. Phys. B **43**, 144008 (2010).
[8] P. Beiersdorfer, J. K. Lepson, M. B. Schneider, and M. P. Bode, Phys. Rev. A **86**, 012509 (2012).
[9] M. D. Rosen, P. L. Hagelstein, D. L. Matthews, E. M. Campbell, A. U. Hazi, B. L. Whitten, B. MacGowan, R. E. Turner, R. W. Lee, G. Charatis, G. E. Busch, C. L. Shepard, P. D. Rockett, and R. R. Johnson, Phys. Rev. Lett. **54**, 106 (1985).
[10] D. L. Matthews, P. L. Hagelstein, M. D. Rosen, M. J. Eckart, N. M. Ceglio, A. U. Hazi, H. Medecki, B. J. MacGowan, J. E. Trebes, B. L. Whitten, E. M. Campbell, C. W. Hatcher, A. M. Hawryluk, R. L. Kauffman, L. D. Pleasance, G. Rambach, J. H. Scofield, G. Stone, and T. A. Weaver, Phys. Rev. Lett. **54**, 110 (1985).
[11] T. Kawachi, K. Murai, G. Yuan, S. Ninomiya, R. Kodama, H. Daido, Y. Kato, and T. Fujimoto, Phys. Rev. Lett. **75**, 3826 (1995).

[12] B. Rus, C. L. S. Lewis, G. F. Cairns, P. Dhez, P. Jaeglé, M. H. Key, D. Neely, A. G. MacPhee, S. A. Ramsden, C. G. Smith, and A. Sureau, Phys. Rev. A **51**, 2316 (1995).
[13] M. S. Bentotoche, M. K. Inal, and M. Benmouna, J. Phys. B **51**, 035701 (2018).
[14] G. Del Zanna and Y. Ishikawa, Astron. Astrophys. **508**, 1517 (2009).
[15] P. Beiersdorfer, E. Träbert, J. K. Lepson, N. S. Brickhouse, and L. Golub, Astrophys. J. **788**, 25 (2014).
[16] Y. Ishikawa, J. M. López Encarnación, and E. Träbert, Phys. Scripta **79**, 025301 (2009).
[17] P. Beiersdorfer, D. Knapp, R. E. Marrs, S. R. Elliott, and M. H. Chen, Phys. Rev. Lett. **71**, 3939 (1993).
[18] W. R. Johnson, J. Sapirstein, and K. T. Cheng, Phys. Rev. A **51**, 297 (1995).
[19] K. T. Cheng and M. H. Chen, Phys. Rev. A **53**, 2206 (1996).
[20] P. Beiersdorfer, A. Osterheld, S. R. Elliott, M. H. Chen, D. Knapp, and K. Reed, Phys. Rev. A **52**, 2693 (1995).
[21] Y. Podpaly, J. Clementson, P. Beiersdorfer, J. Williamson, G. V. Brown, and M. F. Gu, Phys. Rev. A **80**, 052504 (2009).
[22] V. Y. Politov, P. A. Loboda, V. A. Lykov, and J. Nilsen, Opt. Commun. **108**, 283 (1994).
[23] J. Nilsen, P. Beiersdorfer, S. R. Elliott, T. W. Phillips, B. A. Bryunetkin, V. M. Dyakin, T. A. Pikuz, A. Y. Faenov, S. A. Pikuz, S. von Goeler, M. Bitter, P. A. Loboda, V. A. Lykov, and V. Y. Politov, Phys. Rev. A **50**, 2143 (1994).
[24] H. Gordon, M. G. Hobby, and N. J. Peacock, J. Phys. B **13**, 1985 (1980).
[25] W. E. Behring, L. Cohen, G. A. Doschek, and U. Feldman, J. Opt. Soc. Am. **66**, 376 (1976).
[26] B. Edlén, Phys. Scr. **22**, 593 (1981).
[27] W. E. Behring, J. F. Seely, S. Goldsmith, L. Cohen, M. Richardson, and U. Feldman, J. Opt. Soc. Am. **2**, 886 (1985).
[28] U. Feldman, J. O. Eckberg, C. M. Brown, and J. F. Seely, J. Opt. Soc. Am. **6**, 1652 (1986).
[29] M. F. Gu, Can. J. Phys. **86**, 675 (2008).
[30] M. F. Gu, T. Holczer, E. Behar, and S. M. Kahn, Astrophys. J. **641**, 1227 (2006).
[31] V. M. Shabaev, I. I. Tupitsyn, and V. A. Yerokhin, Comput. Phys. Commun. **189**, 175 (2015).
[32] U. I. Safronova, C. Namba, I. Murakami, W. R. Johnson, and M. S. Safronova, Phys. Rev. A **64**, 012507 (2001).
[33] P. Beiersdorfer, A. L. Osterheld, M. H. Chen, J. R. Henderson, D. A. Knapp, M. A. Levine, R. E. Marrs, K. J. Reed, M. B. Schneider, and D. A. Vogel, Phys. Rev. Lett. **65**, 1995 (1990).
[34] P. Beiersdorfer, E. Behar, K. R. Boyce, G. V. Brown, H. Chen, K. C. Gendreau, A. Graf, M.-F. Gu, C. L. Harris, S. M. Kahn, R. L. Kelley, J. K. Lepson, M. J. May, P. A. Neill, E. H. Pinnington, F. S. Porter, A. J. Smith, C. K. Stahle, A. E. Szymkowiak, A. Tillotson, D. B. Thorn, E. Träbert, and B. J. Wargelin, Nucl. Instrum. Methods B **205**, 173 (2003).
[35] P. Beiersdorfer, Can. J. Phys. **86**, 1 (2008).
[36] G. Zschornack, S. Landgraf, F. Grossmann, U. Kentsch, V. Ovsyannikov, M. Schmidt, and F. Ullmann, Nucl. Instrum. Methods B **235**, 160 (2005).
[37] F. S. Porter, B. R. Beck, P. Beiersdorfer, K. R. Boyce, G. V. Brown, H. Chen, J. Gygax, S. M. Kahn, R. L. Kelley, C. A. Kilbourne, E. Magee, and D. B. Thorn, Can. J. Phys. **86**, 231 (2008).
[38] F. S. Porter, J. Gygax, R. L. Kelley, C. A. Kilbourne, J. M. King, P. Beiersdorfer, G. V. Brown, D. B. Thorn, and S. M. Kahn, Rev. Sci. Instrum. **79**, 10E307 (2008).
[39] P. Beiersdorfer, G. V. Brown, J. Clementson, M. Frankel, M. F. Gu, S. M. Kahn, R. L. Kelley, C. A. Kilbourne, F. S. Porter, D. B. Thorn, and E. Träbert, J. Phys.: Conf. Ser. **163**, 012021 (2009).
[40] P. Beiersdorfer, E. W. Magee, E. Träbert, H. Chen, J. K. Lepson, M.-F. Gu, and M. Schmidt, Rev. Sci. Instrum. **75**, 3723 (2004).
[41] P. Beiersdorfer, E. W. Magee, G. V. Brown, N. Hell, E. Träbert, and K. Widmann, Rev. Sci. Instrum. **85**, 11E422 (2014).
[42] P. Beiersdorfer, H. Chen, D. B. Thorn, and E. Träbert, Phys. Rev. Lett. **95**, 233003 (2005).
[43] P. Beiersdorfer, E. Träbert, G. V. Brown, J. Clementson, D. B. Thorn, M. H. Chen, K. T. Cheng, and J. Sapirstein, Phys. Rev. Lett. **112**, 233003 (2014).
[44] E. Träbert, P. Beiersdorfer, N. Hell, and G. V. Brown, Phys. Rev. A **92**, 022509 (2015).
[45] G. W. F. Drake, Can. J. Phys. **66**, 586 (1988).
[46] V. A. Yerokhin and V. M. Shabaev, J. Phys. Ref. Data **44**, 033103 (2015).
[47] E. Ferner, Ark. Mat. Astron. Fysik **36A**, 1 (1948).
[48] R. L. Kelly, J. Phys. Chem. Ref. Data **16**, 1 (1987).